Commun. Comput. Phys.
doi: 10.4208/cicp.171214.210715s

Vol. **x**, No. x, pp. 1-22
x 2015

Multiphysics Modeling of Liver Tumor Ablation by High Intensity Focused Ultrasound

Maxim Solovchuk[1,2,*], Tony Wen-Hann Sheu[1,3,*] and Marc Thiriet[4]

[1] *Center of Advanced Study in Theoretical Sciences (CASTS), National Taiwan University.*
[2] *Institute of Biomedical Engineering and Nanomedicine, National Health Research Institutes, No. 35, Keyan Road, Zhunan, Taiwan 35053, Republic of China.*
[3] *Department of Engineering Science and Ocean Engineering, National Taiwan University, No. 1, Sec. 4, Roosevelt Road, Taipei, Taiwan 10617, Republic of China.*
[4] *Sorbonne Universities, UPMC Univ Paris 06, UMR 7598, Laboratoire Jacques-Louis Lions, F-75005, Paris, France.*

Received xxx; Accepted (in revised version) xxx

Abstract. High intensity focused ultrasound is a rapidly developing technology for the ablation of tumors. Liver cancer is one of the most common malignancies worldwide. Since liver has a large number of blood vessels, blood flow cooling can reduce the necrosed volume and may cause regeneration of the tumor to occur. All cancer cells should be ablated without damaging of the critical tissues. Today, treatment planning tools consider liver as a homogeneous organ. This paper is a step towards the development of surgical planning platform for a non-invasive HIFU tumor ablative therapy in a real liver geometry based on CT/MRI image. This task requires coupling of different physical fields: acoustic, thermal and hydrodynamic. These physical fields can influence each other. In this paper we illustrate how a computational model can be used to improve the treatment efficiency. In large blood vessel both convective cooling and acoustic streaming can change the temperature considerably near blood vessel. The whole tumor ablation took only 30 seconds in the considered simulation case, which is very small comparing with the current treatment time of several hours. Through this study we are convinced that high ultrasound power and nonlinear propagation effects with appropriate treatment planning can sufficiently reduce the treatment time.

AMS subject classifications: 80A20, 65Z05, 68U20, 65N06

Key words: Multiphysics and multiscale model, liver tumor, computational surgery, blood flow, focused ultrasound.

*Corresponding author. *Email addresses:* `solovchuk@gmail.com` (M. Solovchuk), `twhsheu@ntu.edu.tw` (T. W.-H. Sheu), `marc.thiriet@inria.fr` (M. Thiriet)

1 Introduction

Liver cancer is the second leading cause of cancer death in men [1,2] and the sixth leading cause among women in the world. In 2008 around 750 000 patients suffered liver disease in the world [2]. At an early stage liver cancer can be successfully treated with surgery or liver transplantation. For a patient diagnosed at an advanced stage of disease fewer surgical options exist. Unfortunately, no more than 20 percent of patients can be treated with the surgery [2, 3]. If liver tumor cannot be surgically removed, patients can choose local ablation, tumor destruction either with radiofrequency (RFA) or percutaneous ethanol injection (PEI), or embolization by blocking or reducing the blood flow to cancer cells in the liver.

High intensity focused ultrasound (HIFU) is a rapidly developing method for the tumor ablation and it can be used when other methods cannot be applied. It has been successfully applied for the treatment of benign and malignant tumors [3–5]. The principles of using focused ultrasound are very similar to the use of magnifying glass to initiate the fire [6]. Ultrasound beam distributed over the transducer surface is focused onto a very small area. Ultrasound energy is transformed into thermal energy and temperature at the focal region can be increased. If the temperature reaches 56^0C just for one second, protein denaturates and causes an irreversible tissue damage [7]. The goal of the treatment is to achieve this temperature (or corresponding thermal dose) in the whole tumor [8]. If ultrasound beam is properly focused to heat the tumor, the intervening tissues between the transducer and the tumor are not damaged. It is a completely non-invasive method and it has fewer complications in comparison with other treatment modalities.

Ultrasound beam should be properly focused to heat the tumor and avoid the damage of the healthy tissues. Focused ultrasound therapy is usually performed with magnetic resonance imaging or diagnostic ultrasound guidance. Focal area of focused ultrasound transducer (about 1-2 cm in length and 1-2 mm in width) is much smaller than the tumor size. Many sonications should be performed in order to ablate the whole tumor. For the safety and efficiency sake there is a cooling between the ultrasound pulses. Usually treatment time takes several hours [9, 10]. Courivard et al. [10] investigated experimentally in vivo liver tissue ablation by focused ultrasound and the average total procedure time was 380 min. Appropriate treatment planning can sufficiently reduce the treatment time and improve the therapy [11, 12]. Computational fluid dynamics plays a key role in the modeling and analysis of biomedical and biological systems, when many physical mechanisms are involved [13–15]. Several parameters can be optimized during treatment planning including ultrasound power, heating time, scanning path.

Usually linear acoustic model is implemented [9] and homogeneous tissue is considered [11] for the planning of tumor ablation. At high intensities nonlinear propagation effects become important. Nonlinear propagation effects can elevate the temperature and reduce the treatment time [16]. However, simulation of nonlinear acoustic field is more expensive comparing with the linear case [17].

One primary problem in the thermal ablation therapy of liver tumor is due to the indispensable heat sink resulting from the blood flow in large blood vessels. Blood flow cooling reduces the necrosed volume, tumor cells close to the blood vessel wall remain viable and tumor can regenerate due to incomplete ablation. In order to ablate the whole tumor close to blood vessel wall higher ultrasound power can be applied. This can lead to the use of redundant ultrasound power and undesirable damage of healthy tissues. Destruction of vessel walls may cause serious bleeding, therefore prior to the treatment both appropriate ultrasound power and sonication path should be planned.

In most of the previous computational studies, liver is considered as a homogeneous tissue, and the amount of dissipated heat is usually estimated by averaging the effect of blood perfusion over all tissues [18]. It is true only for small blood vessels with a diameter $d < 0.5$ mm. Recently, three-dimensional acoustic-thermal-hydrodynamic coupling model has been proposed [16,19,20]. The model includes the nonlinear Westervelt equation, bioheat equations for the perfused tissue and blood flow domains. The nonlinear Navier-Stokes equations are also employed to model the flow in large blood vessels. Focused ultrasound can induce an additional mass flow. This effect is known as acoustic streaming and is taken into account in the present HIFU simulation study. It can enhance blood flow cooling, representing an additional heat sink [19]. In the current study, acoustic streaming velocity magnitude is four times larger than blood flow velocity.

The propagation of ultrasound in the medium is investigated by solving the Westervelt equation [21]. The original Westervelt equation [21] accounts for the full wave diffraction, nonlinearity and thermoviscous dissipative effects [22–24]. However, the dominant part of acoustic absorption of liver tissue and its components results from macromolecular relaxation processes [25]. Therefore relaxation effects can significantly affect the amount of ultrasound energy deposited to the tumor. Pauly and Schwan [25] showed that in the frequency range 1-10 MHz about two-thirds of the total absorption arises at the macromolecular level (relaxation effect), with the remainder caused by thermoviscous effect. Therefore the importance of relaxation effects is addressed in the current work in a patient specific geometry. We will show that relaxation effects can indeed influence the power deposition.

In the present work temperature elevation in liver tumor is considered in a patient specific geometry. Tumor is located close to the portal vein with the diameter about 7 mm. It will be shown that focused ultrasound can be used to safely ablate tumors close to large blood vessels. The results presented in the current work can be further used to construct a surgical planning platform. Numerical simulations performed on a patient specific geometry can play an important role of training medical doctors, predicting and planning the treatment. It will be shown that the treatment time can be sufficiently reduced. In the present study the treatment time for the tumor with the diameter about 2 cm is around 30 seconds, which is quite small comparing with the common treatment time of several hours [9,10].

2 Multiphysics model

Several physical mechanisms are involved in the propagation of ultrasound wave through living tissues. The propagation of ultrasound in the medium is investigated by solving the nonlinear Westervelt equation with relaxation effects being taken into account. The main mechanism of focused ultrasound ablation is thermal coagulation. Therefore the precise temperature modeling is very important for the treatment planning and all involved processes should be taken into account. The thermal field with convection, conduction, heat source terms is considered. Liver gets a blood supply from hepatic and portal veins, and hepatic artery, so the influence of blood vessels on the temperature distribution shall be studied. The three-dimensional (3D) acoustic-thermal-hydrodynamic coupling model is proposed to compute the pressure, temperature, and blood flow velocity.

2.1 Acoustic model

The most two common models for modeling the finite-amplitude nonlinear wave propagation in soft tissues are Westervelt and Khokhlov-Zabolotskaya-Kuznetsov (KZK) equations [21]. Westervelt equation is a full wave equation, which takes into account the effects of diffraction, absorption and nonlinear propagation:

$$\nabla^2 p - \frac{1}{c_0^2}\frac{\partial^2 p}{\partial t^2} + \frac{\delta}{c_0^4}\frac{\partial^3 p}{\partial t^3} + \frac{\beta}{\rho_0 c_0^4}\frac{\partial^2 p^2}{\partial t^2} = 0. \tag{2.1}$$

In the above, p is the sound pressure, β $(\equiv 1+\frac{B}{2A})$ the coefficient of nonlinearity, and δ the diffusivity of sound resulting from fluid viscosity and heat conduction. The first two terms describe the linear lossless wave propagating at a small-signal sound speed. The third loss term is due to thermal conductivity and fluid viscosity. The last term accounts for acoustic nonlinearity which can affect thermal and mechanical changes within the tissues [26].

KZK equation is the simplified form of Westervelt for directional sound beams. If the retarded time $t_{KZK} = t - z/c_0$ is introduced and the directional sound beam is considered, the Westervelt equation can be transformed to the KZK equation:

$$\frac{\partial^2 p}{\partial z \partial t_{KZK}} - \frac{c_0}{2}\nabla_\perp^2 p - \frac{\delta}{2c_0^3}\frac{\partial^3 p}{\partial t_{KZK}^3} = \frac{\beta}{2\rho_0 c_0^3}\frac{\partial^2 p^2}{\partial t_{KZK}^2}, \tag{2.2}$$

where $\nabla_\perp^2 = \frac{\partial^2}{\partial x^2} + \frac{\partial^2}{\partial y^2}$ is a Laplacian that operates in the plane perpendicular to the axis of the beam.

Introduction of retarded time coordinate allows to sufficiently reduce simulation time for the KZK equation in comparison with the full wave Westervelt equation [27]. As a result, it is more widely used. However KZK equation has several limitations, that don't exist in full wave Westervelt equation. First, effects of reflection and scattering are not

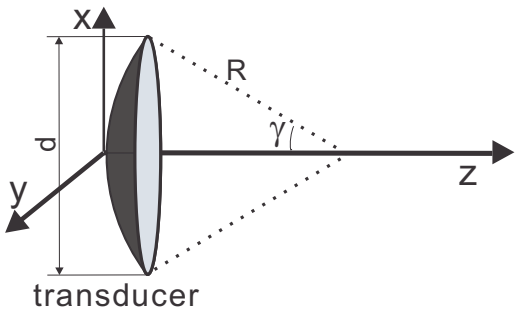

Figure 1: Dimensions and coordinates.

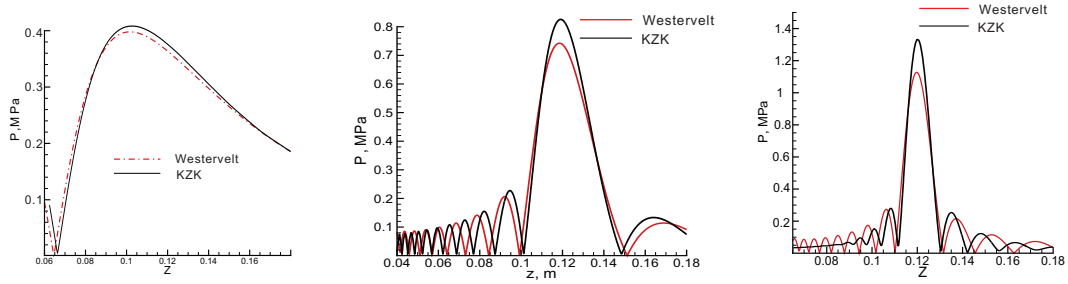

(a) (b) (c)

Figure 2: The comparison of the predicted pressures along acoustic axis for the KZK and Westervelt equations for different apertures angles. (a) aperture angle is 9.6° (aperture diameter $d=4$ cm, focal radius $R=12$ cm); (b) aperture angle $\gamma=19.4°$ ($d=8$ cm, $R=12$ cm); (c) aperture angle $\gamma=30°$ ($d=12$ cm, $R=12$ cm).

taken into account. Second, it can be applied only for the transducers with small aperture angles γ, which is illustrated in Fig. 1. In Fig. 2 the predicted pressures along acoustic axis for KZK and Westervelt equations are presented for different transducer aperture angles. For small aperture angles there is a very good agreement between both acoustic models (Fig. 2(a)). For large aperture angles ($>16°$) the disagreement between two models is large. In our study we consider the transducer with the aperture angle being equal to 30°, therefore Westervelt equation has been chosen.

The traditional Westervelt equation (2.1) was derived for thermoviscous fluid. Attenuation of thermoviscous fluid has the following form:

$$\alpha=\alpha_0\left(\frac{f}{f_0}\right)^2, \tag{2.3}$$

where α_0 is the attenuation at the fundamental frequency f_0. However, in real tissues

$$\alpha=\alpha_0\left(\frac{f}{f_0}\right)^\eta, \tag{2.4}$$

where $\eta=1.0\sim1.4$. In order to take correct attenuation law into account, relaxation effects

should be considered. The generalized Westervelt equation can be written as the coupled system of two partial differential equations given below [16]

$$\nabla^2 p - \frac{1}{c_0^2}\frac{\partial^2 p}{\partial t^2} + \frac{\delta}{c_0^4}\frac{\partial^3 p}{\partial t^3} + \frac{\beta}{\rho_0 c_0^4}\frac{\partial^2 p^2}{\partial t^2} + \sum_i P_i = 0, \tag{2.5a}$$

$$\left(1+\tau_i\frac{\partial}{\partial t}\right)P_i = \frac{2}{c_0^3}c_i\tau_i\frac{\partial^3 p}{\partial t^3}, \tag{2.5b}$$

where τ_i is the relaxation time and c_i is the small signal sound speed increment for the i-th relaxation process. The new auxiliary variable P_i takes into account relaxation effects. In the present paper two relaxation processes ($i=2$) were considered. Unknown relaxation parameters were calculated by minimizing the mean square error between the linear attenuation law and relaxation model [16].

For the linear Westervelt equation the intensity is equal to $I_L = p^2/2\rho c_0$. For the nonlinear case the total intensity is

$$I = \sum_{n=1}^{\infty} I_n, \tag{2.6}$$

where I_n are the corresponding intensities for the respective harmonics nf_0. The ultrasound power deposition per unit volume is calculated as follows

$$q = \sum_{n=1}^{\infty} 2\alpha(nf_0) I_n. \tag{2.7}$$

The absorption in tissue shown above obeys the frequency law $\alpha = \alpha_0 (f/f_0)^\eta$, where $\alpha_0 = 8.1$ Np/m, $\eta = 1.0$ and $f_0 = 1$ MHz [28].

2.2 Energy equation for tissue heating and acoustic streaming hydrodynamic equations

Liver gets a blood supply from hepatic arteries, hepatic veins and portal veins [29, 30]. Blood flow can carry away some of the deposited thermal energy. Tumor cells in perivascular region, as a result, may escape from an externally imposed large heat, leading possibly to a local recurrence. Hence, a mathematical model appropriate for predicting the temperature in tissues must take the heat conduction, tissue perfusion, convective blood cooling, and heat deposition due to an incident wave into account. In the current simulation of thermal field the physical domain has been split into the domains for the perfused tissue and the flowing blood.

In a region free of large blood vessels, the diffusion-type Pennes bioheat equation [18] given below will be employed to model the transfer of heat in the perfused tissue region

$$\rho_t c_t \frac{\partial T}{\partial t} = k_t \nabla^2 T - w_b c_b (T - T_\infty) + q. \tag{2.8}$$

In the above bioheat equation proposed for modelling the time-varying temperature in the tissue domain, ρ, c, k denote the density, specific heat, and thermal conductivity, respectively, with the subscripts t and b referring to the tissue and blood domains. The notation T_∞ is denoted as the temperature at a remote location. The variable w_b ($\equiv 10$ kg/m^3-s) in Eq. (2.8) is the perfusion rate for the tissue cooling in capillary flows. It is noted that the above bioheat equation for T is coupled with the Westervelt equation (2.5) for the acoustic pressure through the power deposition term q defined in Eq. (2.7).

In the region containing large vessels, within which the blood flow can convect heat, the biologically relevant heat source, which is q, and the heat sink, which is $-\rho_b c_b \underline{\mathbf{u}}\cdot\nabla T$, are added to the conventional diffusion-type heat equation

$$\rho_b c_b \frac{\partial T}{\partial t} = k_b \nabla^2 T - \rho_b c_b \underline{\mathbf{u}}\cdot\nabla T + q. \tag{2.9}$$

In the above, $\underline{\mathbf{u}}$ is the blood flow velocity. Owing to the presence of blood flow velocity vector $\underline{\mathbf{u}}$ in the energy equation, a biologically sound model for conducting HIFU simulation should comprise a coupled system of acoustic-thermal-hydrodynamic nonlinear differential equations.

Since there is a heat sink term on the right hand side of Eq. (2.9), the velocity of blood flow must be determined. High-intensity focused ultrasound can induced some additional mass flow (acoustic streaming effect). In the present study effect of acoustic streaming will be taken into account. We consider that the flow in large blood vessels is incompressible $\nabla\cdot\underline{\mathbf{u}} = 0$ and laminar. The vector equation for modeling the blood flow motion in the presence of acoustic stresses is as follows [31]

$$\frac{\partial \underline{\mathbf{u}}}{\partial t} + (\underline{\mathbf{u}}\cdot\nabla)\underline{\mathbf{u}} = \frac{\mu}{\rho}\nabla^2\underline{\mathbf{u}} - \frac{1}{\rho}\nabla\mathbf{P} + \frac{1}{\rho}\underline{\mathbf{F}}. \tag{2.10}$$

In the above, $\mathbf{P}$ is the static pressure, μ ($= 0.0035$ kg/m s) the shear viscosity of blood flow, and ρ the blood density. In Eq. (2.10), the force vector $\underline{\mathbf{F}}$ acting on the blood fluid due to ultrasound is assumed to act along the acoustic axis $\underline{\mathbf{n}}$. The radiation force vector $\underline{\mathbf{F}}$ has the following form [32]

$$\underline{\mathbf{F}}\cdot\underline{\mathbf{n}} = -\frac{1}{c_0}\nabla\vec{I} = \frac{q}{c_0}. \tag{2.11}$$

Thermal dose developed by Sapareto and Dewey [8] will be applied to give us a quantitative relationship between the temperature and time for the tissue heating and the extent of cell killing. Sapareto and Dewey [8] introduced a reference temperature of $43^\circ C$ and proposed the method to convert all thermal exposures to equivalent minutes at this temperature. In focused ultrasound surgery (generally above 50 $^\circ C$), the expression for the thermal dose (TD) can be written as:

$$TD = \int_{t_0}^{t_{final}} R^{(T-43)} dt \approx \sum_{t_0}^{t_{final}} R^{(T-43)} \Delta t, \tag{2.12}$$

where $R=2$ for $T>=43^\circ C$, $R=4$ for $37^\circ C<T<43^\circ C$. The value of TD required for a total necrosis ranges from 25 to 240 min in biological tissues [8]. In the current paper the threshold TD value is chosen to be 240 min. According to this relation, thermal dose resulting from the heating of tissue to $43^\circ C$ for 240 min is equivalent to that achieved by heating it to $56^\circ C$ for one second.

2.3 Solution procedure

Nonlinear Westervelt equation (2.5) is solved using the finite difference method. Discretization of the differential equation is started with the approximation of the temporal derivative $\frac{\partial}{\partial t}P_i^{n+1}$ shown in the second equation of the system (2.5):

$$\frac{\partial}{\partial t}P_i^{n+1}=\frac{1}{2\Delta t}(3P_i^{n+1}-4P_i^n+P_i^{n-1}). \tag{2.13}$$

After algebraic manipulations the second equation in the system (2.5) can be rewritten in the form:

$$P_i^{n+1}=\frac{2}{c_0^3}\frac{c_i\tau_i}{1+1.5\tau_i/\Delta t}\frac{\partial^3 p^{n+1}}{\partial t^3}-\frac{\tau_i}{2\Delta t+3\tau_i}(-4P_i^n+P_i^{n-1}). \tag{2.14}$$

P_ν^{n+1} is then substituted into the first equation of the system (2.5). The resulting equation will be solved implicitly.

Temporal derivatives in Westervelt equation are approximated by the following second order accurate schemes:

$$\left.\frac{\partial^2 p}{\partial t^2}\right|^{n+1}=\frac{2p^{n+1}-5p^n+4p^{n-1}-p^{n-2}}{(\Delta t)^2}, \tag{2.15}$$

$$\left.\frac{\partial^3 p}{\partial t^3}\right|^{n+1}=\frac{6p^{n+1}-23p^n+34p^{n-1}-24p^{n-2}+8p^{n-3}-p^{n-4}}{2(\Delta t)^3}. \tag{2.16}$$

The nonlinear term $\frac{\partial^2 p^2}{\partial t^2}|^{n+1}$ is linearized by the second order accurate relation, leading to

$$\left.\frac{\partial^2 p^2}{\partial t^2}\right|^{n+1}=\frac{\partial}{\partial t}\left(\frac{\partial p^2}{\partial t}\right)\Bigg|^{n+1}=2\frac{\partial}{\partial t}\left(p^n\left.\frac{\partial p}{\partial t}\right|^{n+1}+p^{n+1}\left.\frac{\partial p}{\partial t}\right|^{n}-p^n\left.\frac{\partial p}{\partial t}\right|^{n}\right)$$
$$=2\left(2p_t^n p_t^{n+1}+p^n p_{tt}^{n+1}+p^{n+1}p_{tt}^n-(p_t^n)^2-p^n p_{tt}^n\right). \tag{2.17}$$

The above equations are then substituted into the first equation of Westervelt system (2.5) to get the following Helmholtz equation

$$u_{xx}-ku=f(x). \tag{2.18}$$

Helmholtz equation is then solved using sixth-order accurate scheme which involves only three finite difference stencil points [16]. This scheme development involves relating

the nodal values of derivatives terms, namely, $u^{(2)} \equiv u_{xx}$, $u^{(4)} \equiv u_{xxxx}$ and $u^{(6)}$, to u in order to yield a 3-point stencil implicit scheme as follows:

$$\frac{1}{360}h^6 u_j^{(6)} + \frac{1}{12}h^4 u_j^{(4)} + h^2 u_j^{(2)} = u_{j+1} - 2u_j + u_{j-1}. \tag{2.19}$$

Accuracy of the numerical solutions was examined [16] by comparing them with the known analytical and the numerical solutions obtained by other authors [17, 33]. Good agreement between the measured and numerical results was also obtained [16, 19]. Additional details about the solution of Eq. (2.18) can be found in Ref. [16].

First the acoustic pressure was calculated. The acoustic pressure was calculated only once for a given set of transducer parameters. Afterward ultrasound power deposition in Eq. (2.7) and acoustic streaming force in Eq. (2.11) were determined and stored. Blood flow velocity was computed from Eq. (2.10) at every time step with the acoustic streaming effect being taken into account and then substituted to the bioheat equation (2.9). With the known blood flow velocities and power deposition terms, temperatures in blood flow domain and in liver were calculated. Initially, we consider that the temperature is equal to 37°C. On the outer boundaries of computational domain a constant temperature of 37°C was prescribed. Temperature continuity at the fluid-solid interface is imposed as that applied to a conjugate heat transfer problem. The interface boundary condition takes into account the thermal conduction in liver and convection in blood vessel domain. The three-dimensional problem is analyzed using finite-volume method. A detailed description of the solution procedures can be found in our previous articles [16, 19, 20]. The present 3D computational model was validated by comparing our simulated results for the temperature field, with and without flow, with the experimental results of Huang et al. [24]. The computational model for the prediction of acoustic streaming field was validated by comparing the results with those of Kamakura et al. [31]. Temperature elevation by HIFU in ex-vivo porcine muscle was also studied experimentally by MRI and numerically [34]. We demonstrated that for peak temperatures below 85-90°C numerical simulation results are in excellent agreement with the experimental data in three dimensions. Both temperature rise and lesion size can be accurately predicted. For peak temperatures above 85-90°C "preboiling" or cavitation activity appears and lesion distortion starts, causing a small discrepancy between the measured and simulated temperature rises.

2.4 Patient specific geometry

The present numerical experiments are carried out in a patient-specific liver model. This three-dimensional model was reconstructed was reconstructed from CT images as shown in Fig. 3. Focused ultrasound transducer is located outside of the patient as shown in Fig. 3. There is a water layer between the transducer and skin. In this study the single element HIFU transducer is used with an aperture of 12 cm and a focal length of 12 cm, frequency 1 MHz. The solid tumor was assumed to be exposed to a 0.4 s ultrasound.

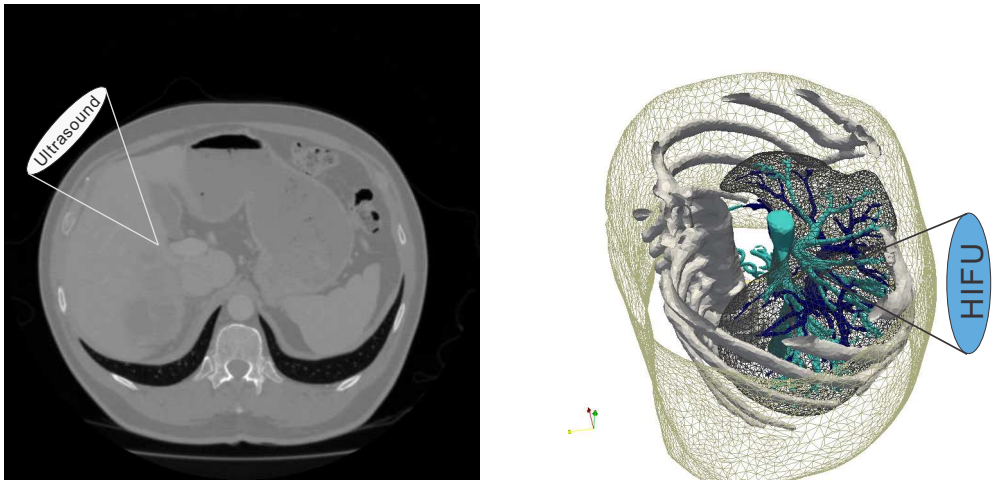

Figure 3: (a) CT image of the upper abdomen for demonstrating the schematic of the treatment. Focused ultrasound transducer is located outside of the patient. There is a water layer between the transducer and skin, penetration depth is 90 mm. (b) Patient specific 3D geometry reconstructed from CT images.

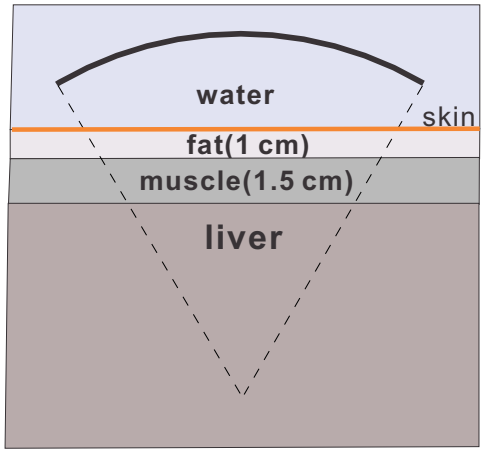

Figure 4: Schematic of the computational domain for showing different layers. Penetration depth is 90 mm. Ultrasound beam propagates through 2 mm of skin, 10 mm of fat and 15 mm of muscle layer.

From the CT image, it was found that ultrasound beam propagates through 2 mm of skin, 10 mm of fat and 15 mm of muscle layer (schematic in Fig. 4). The total penetration depth is about 90 mm.

The reconstructed mesh for the hepatic vein, portal vein and liver is presented in Fig. 5. The total number of tetrahedral elements used in this study is 1.5 million. In the tumor, the refined grids were generated with a mesh length 0.2 mm.

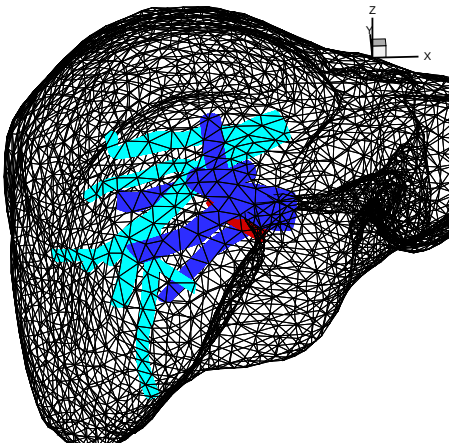

Figure 5: Mesh of the liver with a tumor (red), hepatic (light blue) and portal (dark blue) veins.

3 Results

3.1 Ultrasound propagation through layered tissue

For a successful application of focused ultrasound therapy it is necessary to deliver certain amount of ultrasound energy to a certain location. Numerical simulation may help to choose appropriate transducer parameters and sonication path in order to successfully ablate the tumor and avoid undesirable side effects. Several factors may influence the necrosed volume: penetration depth, sonication time, transducer geometry, ultrasound energy. Ultrasound beam propagates through many tissues on the way from the transducer to the targeted area. In our previous studies [19,23] it was assumed that ultrasound beam propagates entirely in liver, relaxation effects were not considered. In the present paper we are going to consider propagation of ultrasound beam through layered tissue and investigate the importance of relaxation effects. For a plane ultrasound wave, ultrasound intensity is decreasing with the propagation distance z as $I = I_0 e^{-2\alpha z}$, where I_0 is initial intensity, and z is the distance from the transducer. Therefore for a larger penetration depth case it will be necessary to apply higher ultrasound power. Tissue properties may slightly differ from patient to patient, making the treatment planning more complicated. Some tissues, breast for example, are inhomogeneous because of inclusion of fat and connective tissues. Tissue inhomogeneities may distort the focal region and make the prediction of temperature in the focal region very difficult. The schematic of the treatment in the current study is presented in Fig. 3. Tissues are considered to be homogeneous in the present study. Tumor is located below the rib cage, therefore the rib cage is not taken into account in the current study. Acoustic and thermal properties of tissues are summarized in Table 1. It can be seen that fat has a lower absorption and a lower speed of sound comparing with other soft tissues.

Table 1: Acoustic and thermal properties for different tissues.

Tissue	$c_0\ (\frac{m}{s})$	$\rho\ (\frac{kg}{m^3})$	$c\ (\frac{J}{kgK})$	$k\ (\frac{W}{mK})$	$\alpha\ (\frac{Np}{m})$	β
Water	1520	1000	4200	0.6	0.026	3.5
Skin/CT	1540	1100	-	-	16	4.9
Fat	1430	910	-	0.24	7	6.5
Muscle	1560	1050	3700	0.51	9	4.5
Liver	1570	1055	3600	0.51	8.1	4.5
Blood	1540	1060	3770	0.53	1.5	4.0

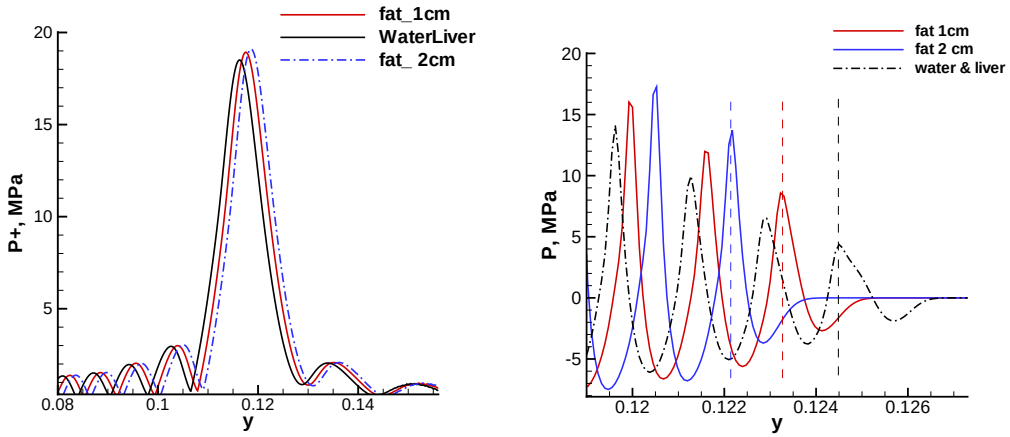

Figure 6: The predicted positive pressures (left) and instantaneous pressures (right) along the acoustic axis. Three cases are considered: 1) thickness of fat layer is 1 cm; 2) thickness of fat layer is 2 cm; 3) propagation only through water and liver. For the three cases under investigation the thickness of water layer and the penetration depth are the same.

In Fig. 6 positive pressures and instantaneous pressures are presented along the acoustic axis for three different cases. For all three cases penetration depth (the total thickness of all soft tissues) is the same. The predicted power depositions are presented in Fig. 7. Due to different attenuations of tissues there is a small difference in the amplitude. Fat has a low propagation speed, therefore when fat layer is included in the simulation focal point is several mm shifted away from the transducer.

3.2 Importance of relaxation and nonlinear effects

The original Westervelt equation was derived for thermoviscous fluids. The attenuation in a thermoviscous fluid depends on the frequency squared. However, in tissues attenuation depends linearly on frequency. To get a correct absorption law relaxation processes should be taken into account. Relaxation refers to the finite time required for a medium

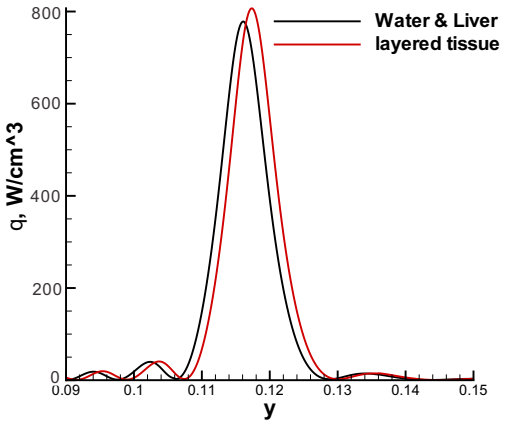

Figure 7: The predicted power depositions along the acoustic axis for the two simulation cases: (1) ultrasound beam propagates only through liver and water; (2) ultrasound beam propagates through layered tissues as shown in Figs. 3(a) and 4.

to reach equilibrium in a new thermodynamic state produced by a change in one or more of the state variables. Several internal processes may contribute to the time required to reach equilibrium: chemical reaction, phase transition, and molecular vibration. Relaxation is accompanied by energy dissipation and introduces dispersion. In the current work two relaxation processes are considered. The absorption coefficient is written in the following form [16]

$$\alpha_n = \alpha_{TV}\omega_n^2 + \frac{1}{c_0^2}\frac{c_1\tau_1\omega_n^2}{1+(\omega_n\tau_1)^2} + \frac{1}{c_0^2}\frac{c_2\tau_2\omega_n^2}{1+(\omega_n\tau_2)^2}. \tag{3.1}$$

There are five unknown parameters α_{TV}, c_1, τ_1, c_2, τ_2 shown in Eq. (3.1). α_{TV} is the absorption coefficient when only thermal and viscous effects are considered. These parameters were calculated by minimizing a mean square error [35] between the tissue attenuation in Eq. (2.4) and relaxation model (3.1) over the frequency band of 500 kHz to 20 MHz. These calculated parameters are $\tau_1 = 2.3369*10^{-6}/2\pi$ s, $\tau_2 = 2.3519*10^{-7}/2\pi$ s, $\alpha_{TV} = 3.0407*10^{-13}$ Np/m/Hz^2, $c_1 = 5.3229$ m/s, $c_2 = 4.3323$ m/s. The diffusivity of sound is $\delta = 2c_0^3\alpha_{TV}/\omega_0^2$.

The predicted linear and nonlinear pressures and power depositions along the acoustic axis calculated with and without relaxation effects being taken into account are presented in Fig. 8. When relaxation effects are taken into account, the peak positive pressure has the largest value. The peak negative value, vise versa, has the smallest absolute value. For both nonlinear cases with and without relaxation effect the peak positive pressure is larger comparing with the linear case. We can see in Fig. 8(b) that relaxation and nonlinear propagation effects enhance power deposition in the focal region and lead to the enhanced heating.

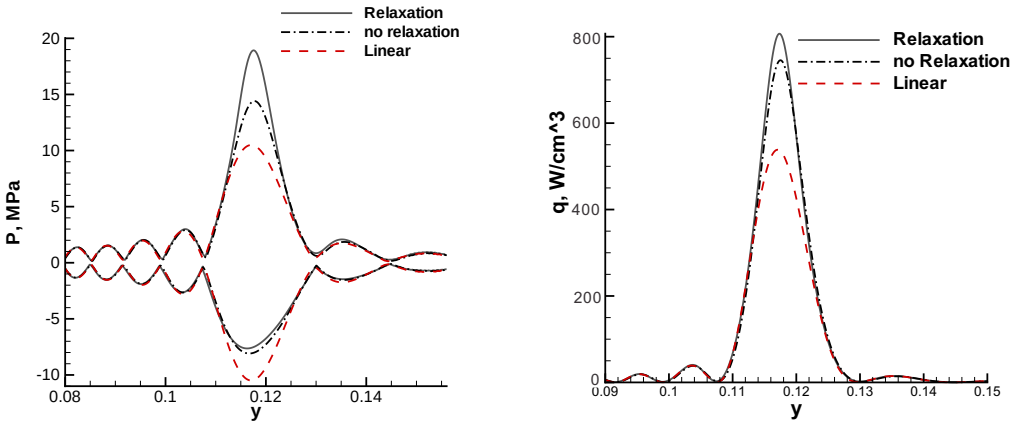

Figure 8: The predicted linear and nonlinear pressures (a) and power depositions (b) along the acoustic axis calculated with and without relaxation effects being taken into account.

3.3 Modeling on liver tumor ablation

In the present section we are going to present numerical results for a patient specific liver model. For the treatment of the whole tumor many sonications should be performed. In the beginning we will consider single sonication. First we are going to investigate the effect of acoustic streaming. Acoustic streaming is considered as a second order physical effect in the HIFU therapy and it is usually neglected. To investigate the importance of acoustic streaming effect during a thermal therapy, we have plotted in Figs. reffig:ASportalVein and 10 the velocity profiles at different cutting planes in portal venous network with and without acoustic streaming effect. Maximum velocity magnitudes in the portal vein for the cases considered with and without acoustic streaming are 37 and 7 cm/s, respectively. Acoustic streaming increases the velocity magnitude by more than four times. This will increase the blood flow cooling and decrease the temperature rise [16, 19]. In Table 2 the predicted mass fluxes at different branches of the portal vein, schematic in Fig. 9(a), are presented with and without acoustic streaming. The mass fluxes at branches 2 and 4 are increased more than twice, the mass flux at branch 3 is decreased by seven times. Hence, acoustic streaming can lead to considerable mass flux redistribution among different branches. This effect can be used to control drug delivery.

Table 2: Acoustic streaming effect on blood mass flow (10^{-3} kg/s) distribution among different branches (B) of the portal vein marked in Fig. 9(a).

Branches	B1	B2	B3	B4	B5	B6	Inlet
Without AS	3.3	0.58	0.53	1.5	1.28	1.13	8.32
With AS	2.2	1.27	0.07	3.3	0.69	0.76	8.32
Difference (%)	-32	+120	-87	+121	-46	-33	

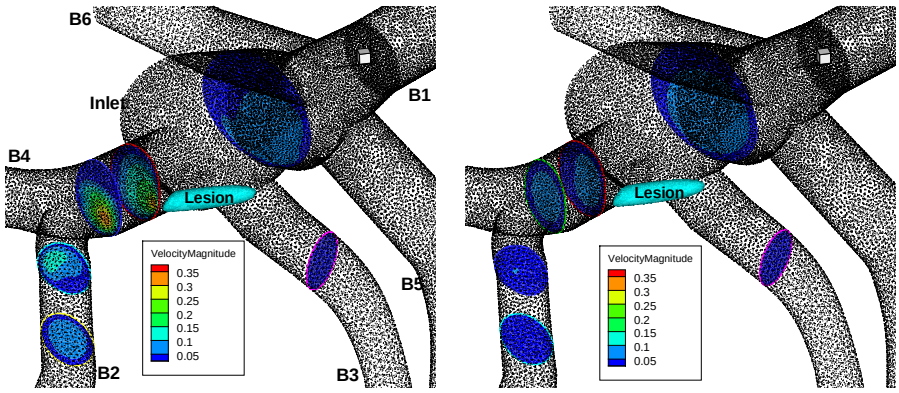

Figure 9: The predicted velocity profiles at different cutting planes in portal venous network when acoustic streaming effect is either taken into account (a) or not (b), lesion is drawn with light blue.

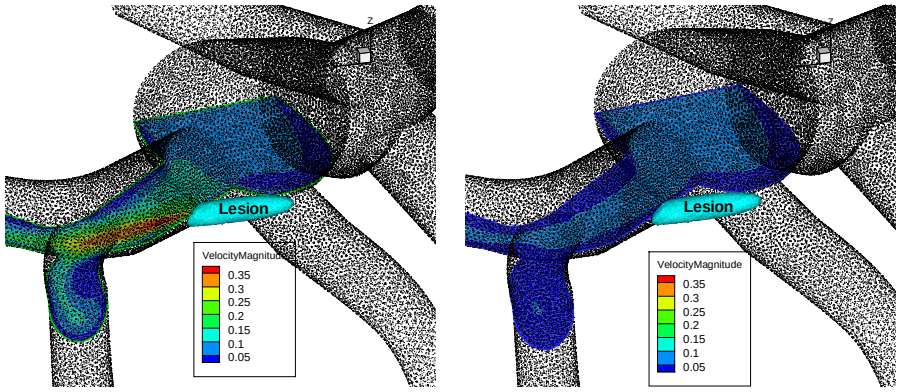

Figure 10: The predicted velocity profiles at the cutting plane $z=0.16$ m (focal plane) in portal venous network when acoustic streaming effect is either taken into account (a) or not (b), lesion is drawn with light blue. Maximum velocities are 0.37 in (a) and 0.07 m/s in (b).

The simulated temperature contours in tumor and in portal vein at the cutting plane $z=0.16$ are presented in Fig. 11 at time $t=0.4$ s (end of sonication). The temperature 56°C can be achieved on the blood vessel wall, therefore tumor close to blood vessel can be ablated. There is a very sharp temperature gradient near the blood vessel wall. We can see a strong asymmetry in the lesion shape due to blood flow cooling. The temperature inside the blood vessel remains almost unchanged except in the boundary layer close to the focal point.

Multiple sonications should be performed for the ablation of the whole tumor. In the current paper the thermal dose (described in Eq. (2.12)) equal to 240 minutes is chosen as a criterion for the tissue necrosis. Tissues temperatures below 100°C are considered. During focused ultrasound ablation of tumors close to the blood vessel wall in moderate intensity regime investigated in Ref. [19] a small layer of cancerous cells remains viable and can cause regeneration of the tumor. Therefore high ultrasound power and short

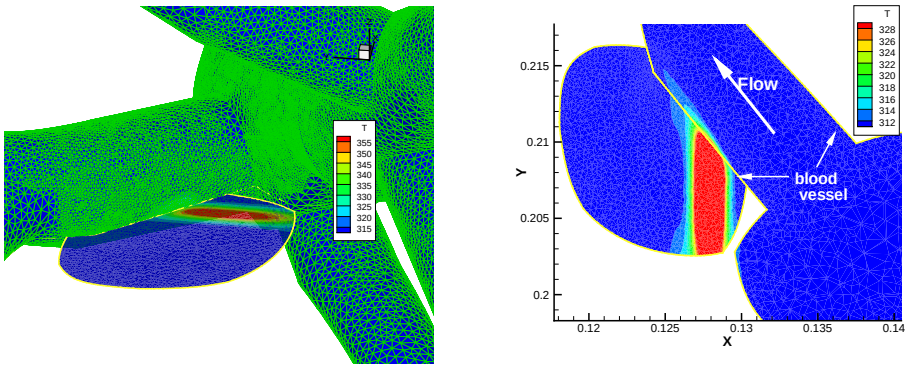

Figure 11: The predicted temperature contours in tumor and in portal vein at the selected cutting plane z=0.16 m for the case with sonication time 0.4 s.

sonication time were applied for the layers close to blood vessel wall in the current study (see Fig. 12(e)). Lower ultrasound power was used for the layers away from the blood vessel wall. Two ultrasound powers 240 and 807 W/cm^3 have been applied for the ablation. The lesion width is about 2.2 cm, the gap between sonications equal to 1.9 cm has been chosen, in order to achieve complete ablation of the tumor. The treatment is performed layer by layer. There are 12 layers in the current tumor. Sonication time at ultrasound power 807 W/cm^3 is 0.4 s for the first layer and 0.35 s for the second and following layers. The distance between the focal point and the blood vessel wall has been adjusted so as to reach the temperature 56 °C on the blood vessel wall. Lower ultrasound power 204 W/cm^3 with average single sonication time 0.55 s has been used for the layers away from the blood vessel wall. It took only 2.7 seconds to ablate the first layer. In Fig. 12 the predicted necrosed volumes after the ablation of the first, second, fourth and sixth layers are presented. The predicted necrosed volume for the whole tumor ablation is presented in Fig. 15. The total treatment time is only 30 seconds. Comparing with the treatment time of several hours we can see that computational fluid dynamics can sufficiently reduce the treatment time and improve the quality of treatment.

In Fig. 12(d) the predicted necrosed volume is bigger than the tumor. In Figs. 12(a)-(d) we can see that with increase of time larger area of healthy tissue is necrosed because of thermal diffusion from the nearby hot spots. Ablation of small part of healthy tissue prevents regeneration of the tumor and does not affect the safety of the treatment. Normally during any cancer treatment, a layer of normal tissue surrounding a tumor (margin) is also ablated along with the tumor. This margin is usually no less than 1 cm [36].

In Fig. 13 the predicted temperature contours in liver, tumor and portal vein are presented at the selecting cutting plane $z=0.16$ m are presented at $t=0.4$ s after single sonication. As a first approximation we can estimate the necrosed area as an area with the temperature higher than 56 °C. The necrosed area has an ellipsoidal shape. The necrosed area will increase due to the thermal diffusion with time. For the correct prediction of the necrosed area the thermal dose should be calculated, which takes into account combined

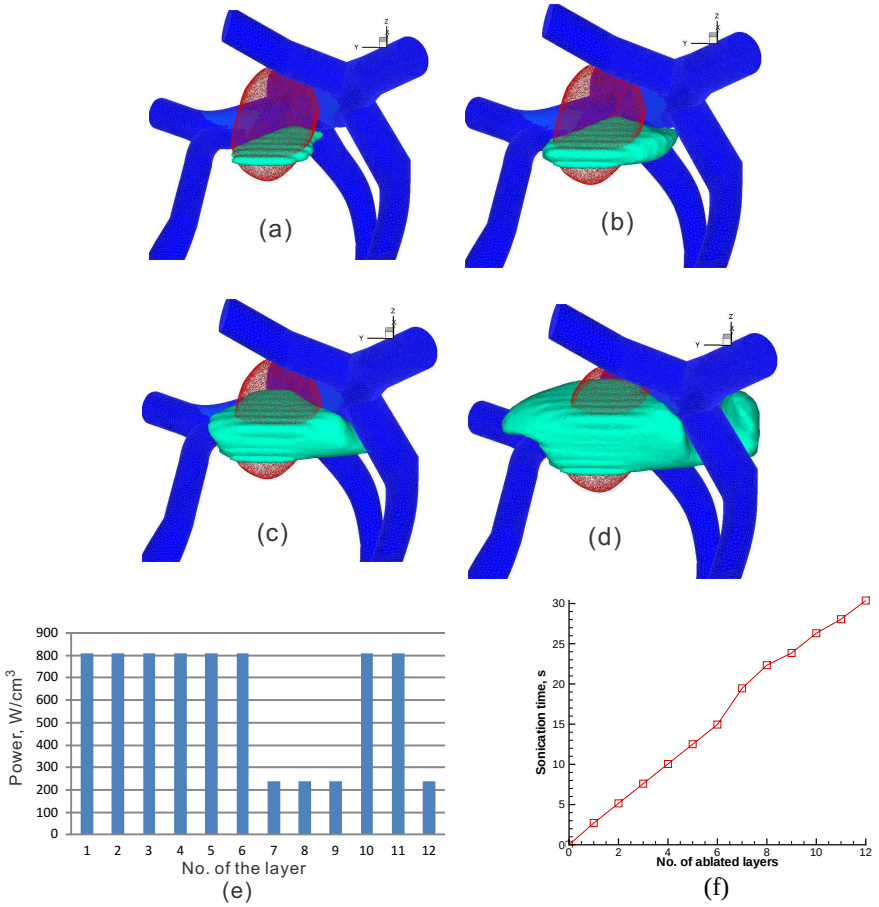

Figure 12: Illustration of the first (a), second (b), fourth (c) and sixth (d) layers ablation. The predicted necrosed volume (light blue) in the tumor (red) close to portal vein (dark blue); (e) ultrasound power at different layers; (f) sonication time as function of the ablated layers number.

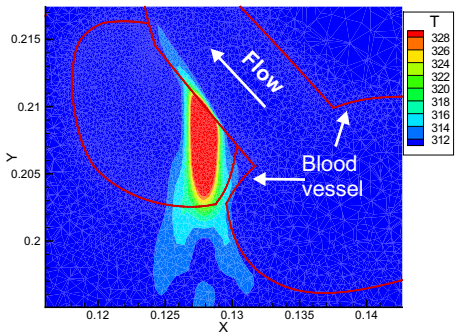

Figure 13: The predicted temperature contours in liver and in portal vein at the selected cutting plane $z=0.16$ m for the case with sonication time 0.4 s.

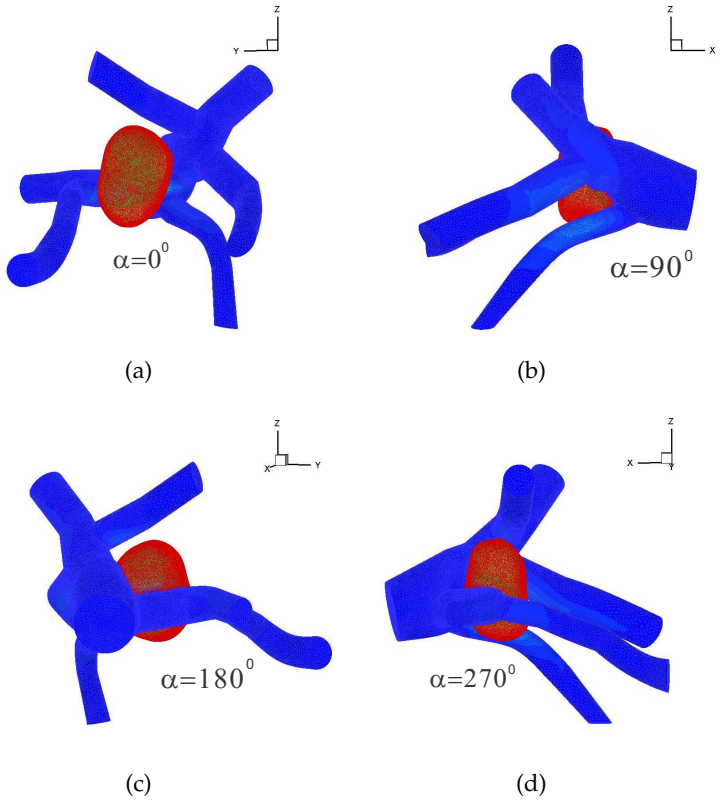

Figure 14: The geometry of the portal vein and tumor at different angles of view.

effect of different sonications. Sonications from different layers will overlap each other and cause the growth of the necrosed area, which can be seen in Fig. 12.

Usually during focused ultrasound treatment of tumors each ultrasound sonication is followed by a cooling period from 50 seconds to several minutes [9, 10], which can result in a very long treatment time of several hours for a 2-3 cm tumor [10] and can limit the application of HIFU for large volume ablation. In this study we showed that numerical simulations can help to reduce the treatment time from several hours to 30 seconds. A part of healthy liver has been destroyed during the treatment. This area can be reduced following one of the methods proposed recently for uniform tissues without large blood vessels [9,11]. These methods include different scanning pathways, different distances between focal points and motion of transducer. Optimization techniques of HIFU treatment in the presence of blood vessel have not been investigated before and will be performed in the following study. In the presence study the main goal was the theoretical investigation of feasibility of full ablation of tumor close to the large blood vessel without damaging the blood vessel wall.

Zhang et al. [37] investigated experimentally safety and effectiveness of HIFU therapy

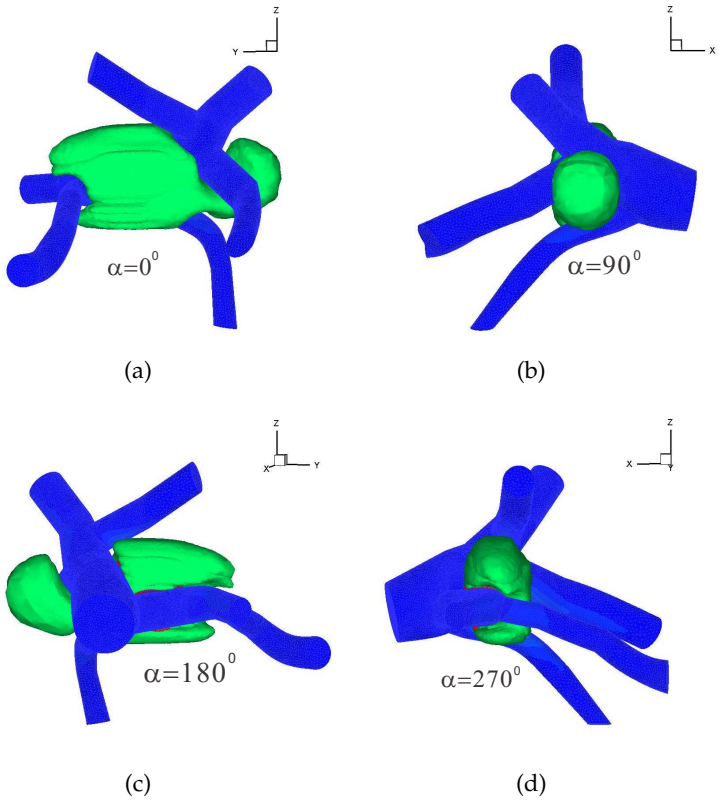

(a) (b) (c) (d)

Figure 15: The predicted necrosed volume (lesion) at different angles of view.

of liver tumors close to major hepatic veins. After a single session of HIFU treatment, the rate of complete necrosis was only about 50%, which is not satisfactory. Lack of a complete response can be attributed to the large tumor size and the cooling effect in large vessels. We showed that computational fluid dynamics can help in the improvement of the efficiency of the treatment.

Comparing with conventional treatment modalities, such as open surgery, radio- and chemotherapy, focused ultrasound therapy is fully non-invasive method and has fewer complications after treatment. Because of non-invasive nature of the method it can be repeated many times. The common adverse effect during the treatment is skin burn. The skin at the sonication site must be hair free and gel should be placed in order to reduce reflection from the skin. Another problem is associated with the beam distortion when ribs lie on the propagation path of focused ultrasound. In the current paper the tumor was located below the rib cage. In general case it is necessary to avoid ribs on the ultrasound way to the target. Reverse time method can be used in order to avoid defocusing of ultrasound beam and overheating of the ribs [3].

Construction of surgical planning platform is a multiple discipline research work, that

includes several tasks:

1. Preprocessing: acquisition of patient specific images (CT or MRI), image segmentation and mesh generation.
2. Simulation: construction of a multiphysics mathematical model; accurate prediction of equations.
3. Calibration of the model: experimental validation of the acoustic, thermal, hydrodynamic fields; measurement of tissue properties.
4. Postprocessing (animation of the three-dimensional results) and analysis.

All four tasks have been accomplished in the current study for one patient. We are working currently toward the construction of surgical planning platform. Simulation results can help to optimize an appropriate set of sonication time, ultrasound power and focal point location.

4 Conclusion

The proposed three dimensional physical model for HIFU study was conducted in an image-based liver geometry. Nonlinear Westervelt equation was considered in this study with relaxation effects being taken into account. It was shown that relaxation effects can affect the temperature distribution. During the treatment planning, the effect of blood flow cooling is not usually taken into account. In the present work we showed, on the contrary, that both blood flow cooling and acoustic streaming effects can significantly affect the treatment and both of them should be taken into account. At high intensities the effect of cooling by acoustic streaming can prevail over convective cooling in large blood vessel. It was also shown that tumors near the blood vessel wall can be ablated without damaging blood vessel wall. These results can be further used to construct a surgical planning platform for a non-invasive HIFU tumor ablating therapy in real liver geometry from CT or MRI image and can lead in the future to a substantial improvement of the focused ultrasound ablation of liver tumor. The presented model can be used in planning tools for the thermal ablation of tumor in other organs and is also applicable to acoustic hemostasis treatment [38].

Acknowledgments

The authors would like to acknowledge the financial support from the Center for Advanced Study in Theoretical Sciences (CASTS) and from the National Science Council of Republic of China under Contract No. NSC102-2811-M-002-125. It was partly supported by NHRI's project BN-104-PP-08. A patient-specific liver geometry in Figure 1 was provided by IRCAD (France).

References

[1] J. S. Huang, D. A. Gervais, P. R. Mueller, Radiofrequency ablation: Review of mechanism, indications, technique, and results, Chinese J. Radiology 26 (2001), 119-134.

[2] Global cancer facts and figures. American Cancer Society, Atlanta, GA 2011. Available from: http://www.cancer.org/Research/CancerFactsFigures/GlobalCancer FactsFigures/global-facts-figures-2nd-ed.

[3] J. F. Aubry, K. B. Pauly, C. Moonen, G. Haar, M. Ries, R. Salomir, S. Sokka, K. M. Sekins, Y. Shapira, F. Ye, H. Huff-Simonin, M. Eames, A. Hananel, N. Kassell, A. Napoli, J. H. Hwang, F. Wu, L. Zhang, A. Melzer, Y. Kim. The road to clinical use of high-intensity focused ultrasound for liver cancer: technical and clinical consensus. J. of Therapeutic Ultrasound (2013), 1:13.

[4] Y. F. Zhou, High intensity focused ultrasound in clinical tumor ablation, World J. Clin. Oncol, 2 (2011), 8-27.

[5] T. A. Leslie and J. E. Kennedy, High intensity focused ultrasound in the treatment of abdominal and gynaecological diseases, Int. J. Hyperthermia 23 (2007) 173-182.

[6] Y. S. Kim, R. Hyunchul, M. J. Choi, H. K. Lim, D. Choi, High-intensity focused ultrasound therapy: an overview for radiologists, Korean J Radiol., 9 (2008), 291-302.

[7] N. T. Wright, J. D. Humphrey, Denaturation of collagen via heating: an irreversible rate process, Annu. Rev. Biomed. Eng., 4 (2002), 109-128.

[8] S. A. Sapareto, W. C. Dewey, Thermal dose determination in cancer therapy, Int. J. Radiat. Oncol. Biol. Phys. 10(6) (1984) 787-800.

[9] J. Coon, A. Payne, R. Roemer, HIFU treatment time reduction in superficial tumours through focal zone path selection, Int. J. Hyperthermia, 27(5) (2011), 465-481.

[10] F. Courivaud, A. M. Kazaryan, A. Lund, V. C. Orszagh, A. Svindland, I. P. Marangos, P. S. Halvorsen, P. Jebsen, E. Fosse, P. K. Hol, B. Edwin, Thermal fixation of swine liver tissue after magnetic resonance-guided high-intensity focused ultrasound ablation, Ultrasound in Medicine and Biology, 40 (2014), 1564-1577.

[11] Y. Zhou, Generation of uniform lesions in high intensity focused ultrasound ablation, Ultrasonics, 53 (2013), 495-505.

[12] M. M. Paulides, P. R. Stauffer, E. Neufeld, P. F. Maccarini, A. Kyriakou, R. A. M. Canters, C. J. Diederich, J. F. Bakker, G. C. Van Rhoon, Simulation techniques in hyperthermia treatment planning, International Journal of Hyperthermia, 29 (2013) 346-357.

[13] M. Garbey, R. Salmon, D. Thanoon, B.L. Bass, Multiscale modeling and distributed computing to predict cosmesis outcome after a lumpectomy, Journal of Computational Physics, 244 (2013) 321-335.

[14] Special Issue on Multi-scale Modeling and Simulation of Biological Systems, Journal of Computational Physics, 244 (2013), 1-336.

[15] G.C.Y. Peng, Editorial: what biomedical engineers can do to impact multiscale modeling, IEEE Transactions on Biomedical Engineering, 58 (12, Part 2) (2011), 3440-3442.

[16] M. A. Solovchuk, T. W. H. Sheu, M. Thiriet, Simulation of nonlinear Westervelt equation for the investigation of acoustic streaming and nonlinear propagation effects, J. Acoust. Soc. Am., 134 (2013), 3931-3942.

[17] H. T. O'Neil, Theory of focusing radiators, J. Acoust. Soc. Am. 21(5) (1949) 516-526.

[18] H. H. Pennes, Analysis of tissue and arterial blood temperature in the resting human forearm, J. Appl. Physiol., 1 (1948), 93-122.

[19] M. A. Solovchuk, T. W. H. Sheu, M. Thiriet, W. L. Lin, On a computational study for investi-

gating acoustic streaming and heating during focused ultrasound ablation of liver tumor, J. of Applied Thermal Engineering, 56 (2013), 62-76.
[20] M. A. Solovchuk, T. W. H. Sheu, W. L. Lin, I. Kuo, and M. Thiriet, Simulation study on acoustic streaming and convective cooling in blood vessels during a high-intensity focused ultrasound thermal ablation, Int. J. Heat and Mass Transfer, 55 (2012), 1261-1270.
[21] M. F. Hamilton, D. T. Blackstock, Nonlinear Acoustics, Academic Press, Boston, 1998.
[22] I. Hallaj, R. Cleveland, FDTD simulation of finite-amplitude pressure and temperature fields for biomedical ultrasound, J. Acoust. Soc. Am. 105(5) (1999) L7-L12.
[23] M. A. Solovchuk, T. W.H. Sheu, M. Thiriet, Effects of acoustic nonlinearity and blood flow cooling during HIFU treatment, AIP Conf. Proc., 1503 (2012), 83-88.
[24] J. Huang, R. G. Holt, R. O. Cleveland, R. A. Roy, Experimental validation of a tractable medical model for focused ultrasound heating in flow-through tissue phantoms, J. Acoust. Soc. Am. 116(4) (2004) 2451-2458.
[25] H. Pauly, H. P. Schwan, Mechanism of Absorption of Ultrasound in Liver Tissue, The Journal of the Acoustical Society of America, 50 (1971), 692-699.
[26] M. Bailey, V. Khokhlova, O. Sapozhnikov, S. Kargl, L. Crum, Physical mechanism of the therapeutic effect of ultrasound (A review), Acoust. Physics, 49(4) (2003) 369-388.
[27] E. A. Filonenko, V. A. Khokhlova, Effect of acoustic nonlinearity on heating of biologocal tissue by high-intensity focused ultrasound, Acoust. Physics 47(4) (2001) 468-475.
[28] F. A. Duck, Physical Property of Tissues - A comprehensive reference book, Academic, London, 1990.
[29] M. Thiriet, Biology and Mechanics of Blood Flows. Part I: Biology, Springer, New York, 2008
[30] T. W. H. Sheu, M. A. Solovchuk, A. W. J. Chen, M. Thiriet, On an acoustics-thermal-fluid coupling model for the prediction of temperature elevation in liver tumor, Int. J. Heat and Mass Transfer, 54(17-18) (2011) 4117-4126.
[31] T. Kamakura, M. Matsuda, Y. Kumamoto, M.A. Breazeale, Acoustic streaming induced in focused Gaussian beams, J. Acoust. Soc. Am. 97 (1995) 2740-2746.
[32] W. L. Nyborg, Acoustic Streaming in: Hamilton MF, Blackstock DT (Eds.), Nonlinear Acoustics, (Academic Press, San Diego, 1998), Ch. 7.
[33] D. T. Blackstock, Connection between the Fay and Fubini solutions for plane sound waves of finite amplitude, J. Acoust. Soc. Am., 14 (1966) 1019-1026.
[34] M. A. Solovchuk, S. C. Hwang, H. Chang, M. Thiriet, T. W. H. Sheu, Temperature elevation by HIFU in ex-vivo porcine muscle: MRI measurement and simulation study, Medical Physics, 41 (2014), 052903.
[35] X. Yang, R. O. Cleveland, Time domain simulation of nonlinear acoustic beams generated by rectangular pistons with application to harmonic imaging, J. Acoust. Soc. Am., 117 (2005) 113-123.
[36] T. Leslie, R. Ritchie, R. Illing, G. Ter Haar, R. Phillips, M. Middleton, F. Wu, D. Cranston,. High-intensity focused ultrasound treatment of liver tumours: post-treatment MRI correlates well with intra-operative estimates of treatment volume, The British Journal of Radiology,85 (2012), 1363-1370.
[37] L. Zhang, H. Zhu, C. Jin, K. Zhou, K. Li, H. Su, W. Chen, J. Bai, Z. Wang, High-intensity focused ultrasound (HIFU): effective and safe therapy for hepatocellular carcinoma adjacent to major hepatic veins, Eur. Radiol. 19 (2009) 437-445.
[38] M. A. Solovchuk, T. W. H. Sheu, Computational model for investigating acoustic hemostasis, in proceedings of "Int. Workshop on Computational Science and Engineering" PoS(IWCSE 2013) 019.